

Cite this: DOI: 10.1039/c0xx00000x

www.rsc.org/xxxxxx

## Photoelectron spectroscopy of the model GFP chromophore anion†

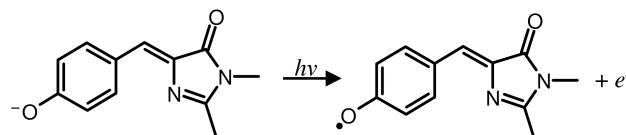
Daniel A. Horke<sup>a</sup> and Jan R. R. Verlet<sup>\*a</sup>

Received (in XXX, XXX) Xth XXXXXXXXX 20XX, Accepted Xth XXXXXXXXX 20XX

DOI: 10.1039/b000000x

5 A photoelectron spectroscopy study of the anionic model chromophore of the green fluorescent protein is presented. From the photoelectron spectra taken at 3.496 eV, 4.62 eV, and 6.15 eV the vertical and adiabatic detachment energies are determined to be  $2.8 \pm 0.1$  eV and  $2.6 \pm 0.2$  eV, respectively. The vertical detachment energy is higher than the  $S_1 \leftarrow S_0$  absorption maximum (2.57 eV) and indicates that the  $S_1$  state is bound with respect to electron detachment in the Franck-Condon region. The photoelectron spectrum taken at 6.15 eV, together with TD-DFT calculations, are used to assign a number of excited states in the neutral radical that correspond to electron loss from occupied orbitals in the anion. The photoelectron spectrum at 2.58 eV shows evidence for electrons formed by thermionic emission, suggesting that internal conversion is the dominant relaxation pathway following  $S_1 \leftarrow S_0$  excitation.

The discovery of fluorescent proteins, and most importantly the green fluorescent protein (GFP), has revolutionised biology through its use as a marker for *in vivo* monitoring of biological processes.<sup>1-4</sup> The optical properties of GFP can be attributed to a chromophore which is based on p-hydroxybenzylidene-2,3-dimethylimidazolinone (HBDI, Fig. 1). The chromophore resides in the  $\beta$ -barrel of the protein and exists in anionic (deprotonated) and neutral forms and is responsible for the two strong absorption bands of the GFP protein. The A band (395 – 397 nm) corresponds to absorption of the neutral chromophore and the B band (470 – 475 nm) is assigned to the anionic chromophore.<sup>5, 6</sup> The anionic form of HBDI is highly fluorescent within the protein (quantum yield  $\Phi_f = 0.79$ ) following  $S_1 \leftarrow S_0$  excitation, whereas the neutral form undergoes ultrafast hydrogen transfer to form the fluorescent anion.<sup>6, 8</sup> In solution, HBDI<sup>-</sup> was found to be virtually non-fluorescent,<sup>9</sup> but the fluorescence returned at temperatures below the glass transition.<sup>10</sup> The differing excited state dynamics are however not surprising given that the absorption spectra also differ between solution and protein. In contrast, for HBDI<sup>-</sup> isolated in the gas-phase, the absorption spectrum appears very similar to that of the protein and this has been accounted for by the exclusion of water around the chromophore in the  $\beta$ -barrel of the protein which presents a solvent-free “gas-phase” like environment.<sup>11, 12</sup> Recent gas-phase experiments on the isolated HBDI<sup>-</sup> have shown that the primary deactivation pathways following excitation to the  $S_1$  excited state are electron detachment and fragmentation, but not fluorescence.<sup>13, 14</sup> However, yet unknown properties of HBDI<sup>-</sup> are



50 Fig. 1 HBDI<sup>-</sup> chromophore and radical formed upon photodetachment.

its vertical and adiabatic detachment energies, which are important to understand the observed decay dynamics and are key benchmark values in current theoretical investigations into the structure and dynamics of the GFP chromophore. Here, these values are experimentally determined using UV photoelectron spectroscopy (Fig. 1).<sup>15, 16</sup>

The experimental setup has been described in detail before, and only a very brief overview is given.<sup>17, 18</sup> HBDI is synthesised according to published methods.<sup>19</sup> Deprotonated HBDI<sup>-</sup> is produced through electrospray ionisation (~1mM in MeOH, pH ~ 10 through addition of NaOH) and introduced into vacuum. Ions are subsequently trapped in a radio frequency ion trap and mass selected by time-of-flight spectroscopy. HBDI<sup>-</sup> is irradiated with 268.1 nm and 201.5 nm laser pulses generated from the third and fourth harmonic respectively, of a commercial femtosecond Ti:Sapphire oscillator and amplifier. Pulses at 480 nm (2.58 eV) are generated by sum-frequency mixing of the fundamental with the signal output from an optical parametric amplifier. This produces pulses of ~ 100 fs duration with a bandwidth of 40 meV. Intensities in the interaction region are  $1.4 \times 10^9$  W cm<sup>-2</sup>,  $2.8 \times 10^8$  W cm<sup>-2</sup> and  $1.6 \times 10^9$  W cm<sup>-2</sup> for the 268.1 nm, 201.5 nm and 480 nm, respectively. We have also recorded the photoelectron spectrum using the 3<sup>rd</sup> harmonic from a nanosecond Nd:YAG laser (355 nm). Photodetached electrons are collected using a velocity-map imaging setup,<sup>20</sup> and the resultant photoelectron images are deconvoluted using the polar onion-peeling algorithm.<sup>21</sup> A background (laser only) image has been subtracted from the spectra at 4.62 eV and 6.15 eV to remove electrons produced by photoemission from surfaces. The spectrometer and UV photon energies have been calibrated using the known photodetachment from iodide (I<sup>-</sup>) before and after every HBDI<sup>-</sup> image was taken. The spectrometer energy resolution ( $\Delta eKE/eKE$ ) is ~ 5%.

Figure 2 shows photoelectron spectra of HBDI<sup>-</sup>, collected at 3.496 eV (355 nm, Fig. 2(a)), 4.62 eV (268.1 nm, Fig. 2(b)) and 6.15 eV (201.5 nm, Fig. 2(c)). To accurately determine the vertical detachment energy (*VDE*) of HBDI<sup>-</sup> in the gas-phase, care has been taken to avoid any unnecessary heating of the

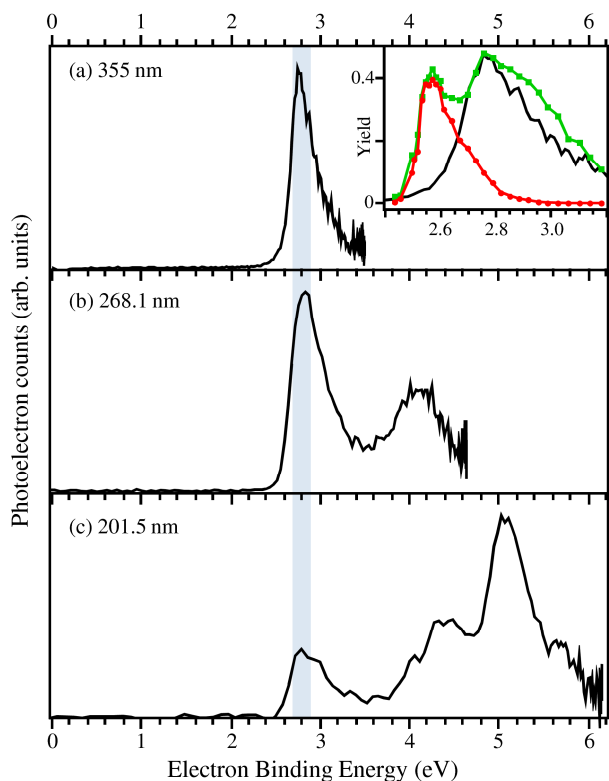


**Fig. 2** Photoelectron spectra of HBDF<sup>-</sup> collected at photon energies (a) 3.496 eV (355 nm), (b) 4.62 eV (268.1 nm) and (c) 6.15 eV (201.5 nm).

The vertical detachment energy is determined as  $2.8 \pm 0.1$  eV and indicated by the vertical shaded area. The adiabatic binding energy is estimated by extrapolation of the rising edge and is  $\sim 2.6$  eV. Also shown inset in (a) are the fragmentation yield (red circles) and inferred photodetached electron yield (green squares) spectra collected by Forbes and Jockusch.<sup>13</sup>

anions for the spectra shown in Fig. 2(a) and (b). This is controlled via the use of Helium buffer gas in the ion trap and low trapping voltages, leading to ions at approximately room temperature. We determine the *VDE* to be  $2.8 \pm 0.1$  eV for the photoelectron spectra. This is indicated by the shaded area in Fig. 2 and is in excellent agreement with the 6.15 eV photoelectron spectrum shown in Fig. 2(c).

The measured gas-phase *VDE* is significantly higher in energy than the  $S_1 \leftarrow S_0$  absorption maximum, which has been measured to be  $\lambda_{\text{max}} = 482.5$  nm,<sup>13</sup> corresponding to an excitation energy of 2.57 eV. The inset in Fig. 2(a) compares our photoelectron spectrum with the action spectra collected by Forbes and Jockusch, where both the electron yield (circles) and the fragmentation yield (squares) are shown independently.<sup>13</sup> The fragmentation yield shows a single feature peaking at 2.57 eV, while the electron yield shows an almost identical feature as well as an additional feature peaking at 2.76 eV. The feature at 2.57 eV has been assigned to the  $S_1 \leftarrow S_0$  origin, while the separation to the second feature indicates that this corresponds to a vibrational level of the  $S_1$  state.<sup>13</sup> Comparison of the electron yield with our photoelectron spectrum however, shows that position and onset of the second peak in the electron yield correlates remarkably well with the photodetachment onset. Given that this feature is not reproduced in the fragmentation yield channel seems to suggest that the feature around 2.76 eV in the electron yield spectrum is due primarily to direct detachment

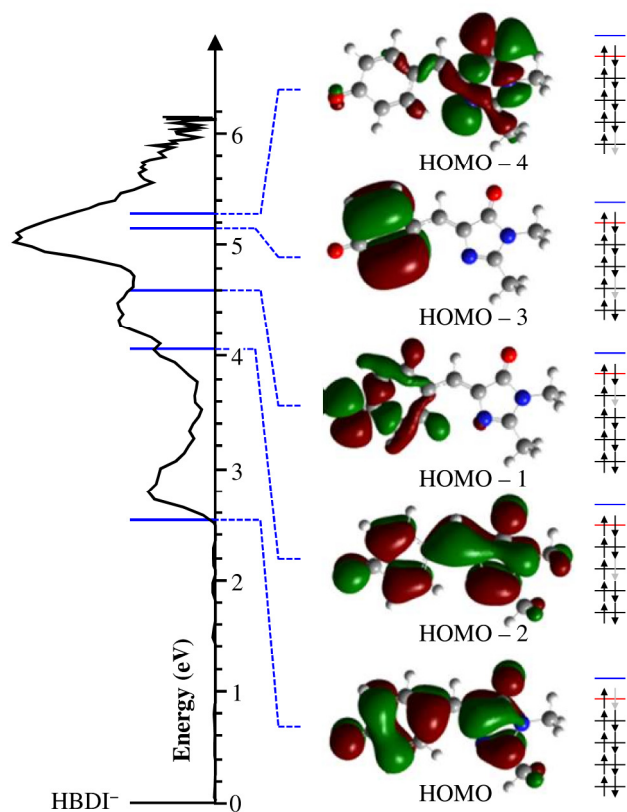
and/or autodetachment into the continuum. Importantly, the correlation between the photoelectron spectrum and the action spectra reinforces the conclusion that the  $S_1$  state origin lies below the *VDE* in the Franck-Condon region

HBDF<sup>-</sup> and other related chromophores have been the subject of a large number of theoretical investigations, both in terms of electronic structure and excited state dynamics, and these have been recently reviewed.<sup>22</sup> The most recent theoretical studies have determined the *VDE* to be 2.54 eV<sup>23,24</sup> and therefore below the  $S_1 \leftarrow S_0$  absorption maximum. Despite the very high level and robustness of the electronic structure calculations employed ( $\pm 0.1$  eV), our experimental determination of the *VDE* relative to the experimentally determined  $S_1 \leftarrow S_0$  origin does not agree with these calculations.

The adiabatic detachment energy can be estimated by linear extrapolation of the rising edge of the photoelectron feature. For all the spectra shown in Fig. 2, this yields  $2.6 \pm 0.2$  eV, which coincides with the maximum of the  $S_1 \leftarrow S_0$  transition.<sup>13</sup> High level theory predicts the adiabatic energy to be 2.39 eV,<sup>23,24</sup> which is significantly lower than the experimental observation. We point out however that the experimental determination of the adiabatic energy is a rather crude estimate and recognise that the spectral onset is at 2.4 eV, although this is in part due to the contribution of hot bands and the resolution of our spectrometer.

The origin of the discrepancy between experiment and high-level theory is not clear. The fact that the 3.496 eV, 4.62 eV and 6.15 eV yield identical *VDE*s and spectral shapes for the detachment feature into  $D_0$  indicates that there are no resonances accessed at these energies. Furthermore, these photon energies are so far above the  $S_1$  that it is inconceivable that the  $S_1$  state is excited upon photodetachment. A key difference between the two is of course that experimentally, HBDF<sup>-</sup> is at a finite temperature. The photoelectron spectra presented in Fig. 2(a) and (b) were obtained for ions that are at approximately 300 K. We can induce significant thermal intra-molecular excitation of the ions by using a heavier buffer gas in the trap.<sup>25</sup> However, even at significantly elevated temperatures, we see no noticeable shift in the *VDE* (see ESI) and the photoelectron spectra appear very similar. Moreover, the extrapolated adiabatic binding energy is likely to be higher when cooled as the presence of hot-bands is reduced. Nonetheless, it would certainly be interesting to obtain a high-resolution photoelectron spectrum of HBDF<sup>-</sup> at cold temperatures.<sup>26</sup> We have also simulated the photoelectron spectrum using structures obtained from our calculations discussed below, but these also do not explain the discrepancy (see ESI).

The photoelectron spectrum shown in Fig. 2(b) also shows the presence of a neutral excited state with an electron binding energy (*eBE*) of  $\sim 4.1$  eV. This is confirmed by the 6.15 eV photoelectron spectrum shown in Fig. 2(c), which reveals a number of additional excited states around *eBE*  $\sim 4.4$  eV and  $\sim 5.1$  eV. To gain some insight into the nature of the observed excited states, we have carried out time-dependent density functional theory (TD-DFT) calculations, utilizing the CAM-B3LYP functional<sup>27</sup> with an augmented, correlation-consistent double-zeta basis set (aug-cc-pVDZ), within the Gaussian09 software suite.<sup>28</sup> The Coulomb attenuated method (CAM) is employed to specifically account for intra-molecular charge

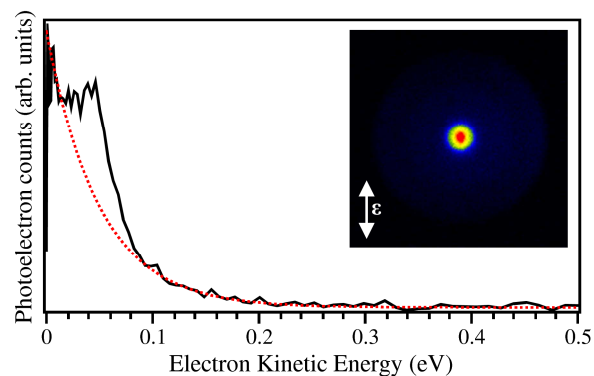


transfer in excited states. All calculations were carried out within  
**Fig. 3** Calculated neutral excited states of the HBDI radical (blue bars) superimposed on photoelectron spectrum of HBDI<sup>-</sup> collected at 6.15 eV (201.5 nm). Shown molecular orbitals (MOs) correspond to those of the anion from which an electron is removed, leading to the corresponding neutral excited states that are accessed upon photodetachment. The electronic configuration of the anion is shown where the grey electron is the one that is removed to form the neutral state. Red level is the highest occupied MO (HOMO) and blue level is the lowest unoccupied MO (LUMO).

the anion optimised geometry (optimised at the CAM-B3LYP/aug-cc-pVDZ level) given that electron detachment is a vertical process.

Fig. 3 shows the location of calculated excited states in the neutral relative to the anion ground state, superimposed on the photoelectron spectrum taken at 6.15 eV. The *VDEs* are calculated as the anion to neutral vertical energy separation, for which the robust literature value of 2.54 eV is used,<sup>23</sup> plus the excitation energy for the corresponding neutral excited state in the anion geometry. The calculated photoelectron peak positions reproduce the observed photoelectron spectrum remarkably well. Assuming that all photodetachment processes have a similar cross-section, then all features of the photoelectron spectrum can be assigned to specific transitions in the neutral.

Analysis of the excited states of the neutral (see ESI for details) reveals that the dominant contribution to the first four excited states can be identified as transitions from successively more bound doubly occupied molecular orbitals (MOs) to the singly occupied highest occupied MO (HOMO) of the neutral radical. The HOMO of the neutral is the same orbital as the HOMO of the anion. The neutral excited states can thus be viewed from the anion's perspective as corresponding to the



removal of an electron from successive MOs in the anion. The 5  
**Fig. 4** Photoelectron spectrum of HBDI<sup>-</sup> collected at 480 nm (2.58 eV), resonant with the S<sub>1</sub> ← S<sub>0</sub> transition. A clear exponential feature at low kinetic energies can be identified (dashed line) and corresponds to thermionic electron loss from the ground state of the anion following internal conversion. Shown inset is the raw photoelectron image, highlighting the production of zero and very low kinetic energy electrons. The arrow indicates the laser polarisation axis,  $\epsilon$ .

highest occupied MOs in HBDI<sup>-</sup> are shown in Fig. 3.

The neutral ground state corresponds to detachment from the HOMO, leaving the neutral with a singly-occupied (radical) HOMO. Although we calculate the *VDE* to be 2.79 eV, in remarkable agreement with experiment, this is significantly higher than previous higher level electronic structure calculations placing the *VDE* at 2.54 ± 0.1 eV.<sup>23</sup> The first neutral excited state, calculated to be 1.54 eV above the neutral ground state, corresponds to detachment from the HOMO - 2 (of the anion). This neutral excited state thus corresponds to the removal of a single electron from that MO. The predicted *VDE* for this feature is 4.08 eV, in good agreement with the experimentally observed electron binding energy at 4.1 eV. Detachment from the HOMO - 1 results in an excited state calculated to lie at an electron binding energy of 4.61 eV, most likely corresponding to the feature measured at 4.4 eV. The next two excited states are calculated to have dominant contributions from excited states corresponding to the removal of an electron from the HOMO - 3 and HOMO - 4 of the anion. These are calculated to lie at electron binding energies of 5.17 and 5.30 eV, respectively. The near degeneracy of these two states accounts for the increased intensity associated with the feature around 5.1 eV, which has approximately doubled with respect to all other photoelectron features. The correlation between experiment and theory provides some confidence that our assignment is correct. This indicates that the photoelectron spectrum at 6.15 eV serves as a sensitive probe for the MOs of the HBDI<sup>-</sup> chromophore that resides in GFP and hence a benchmark for high-level theoretical calculations of the GFP chromophore anion.

We now return to the observation that the experimentally determined *VDE* = 2.8 ± 0.1 eV is higher than the S<sub>1</sub> ← S<sub>0</sub> origin at 482.5 nm (2.57 eV). Their relative values are important in determining the role of autodetachment of HBDI<sup>-</sup> following excitation in the gas-phase. The fact that the *VDE* is higher implies that this autodetachment into the continuum following excitation around 480 nm is not a major decay channel, at least not in the Franck-Condon region. However, the extrapolated adiabatic binding energy suggests that the D<sub>0</sub> state in the neutral

geometry lies at a similar energy as the  $S_1$  origin, and according to calculations it is 0.18 eV below the  $S_1$  maximum.<sup>23</sup> Hence, there may be an energetically accessible continuum for autodetachment following motion on the  $S_1$  state. Indeed, Jockusch and co-workers have shown that following excitation at 480 nm (2.58 eV), both fragments and electrons are produced, as shown inset in Fig 2(a).<sup>14</sup> At higher excitation energy, both direct and autodetachment are clearly accessible channels, based on the comparison of the action and the photoelectron spectra.

To gain some additional insight into the nature of electron emission following excitation to the  $S_1$  state, in Fig. 4 the photoelectron spectrum taken at 480 nm (2.58 eV), is presented. A key observation in this spectrum is the presence of electrons with  $eKE \sim 0$  eV, as highlighted in the photoelectron image inset in Fig. 4. These cannot be generated following direct detachment because the photodetachment cross-section for anions is zero at threshold.<sup>29</sup> These zero- $eKE$  electrons could potentially arise from two processes: (i) autodetachment from the excited state, as described above or (ii) thermionic emission from a hot ground state following internal conversion to the anion ground state.<sup>30-33</sup> Thermionic emission would appear as a falling exponential in the photoelectron spectrum and, between  $0.1 < eKE < 0.2$  eV, there is clear evidence for the tail of such an exponential. The spectral shape,  $I(eKE)$ , of thermionic emission can be crudely modelled using  $I(eKE) = \exp(-eKE/k_B T)$ ,<sup>33, 34</sup> where  $T$  is a measure of the temperature of the ion following internal conversion. A fit with  $T = 575$  K is shown in Fig. 4 (dashed line) indicating that the high  $eKE$  tail is well reproduced by the model. Although this temperature is not very meaningful because there are competing decay mechanisms (specifically fragmentation), the fact that thermionic emission is observed is an important indicator that internal conversion is operative at 480 nm, despite the suggestions in the literature that the  $S_1$  is unbound with respect to detachment.

In addition to thermionic emission, there also appears to be some direct or autodetachment as evidenced by the feature at  $eKE \sim 0.05$  eV. Direct detachment could occur due to the finite bandwidth of our femtosecond laser system (40 meV full width at half-maximum) or the presence of hot bands due to the finite ion temperatures. Alternatively, autodetachment could arise from motion on the excited state and changes in the relative energy of the  $S_1$  and  $D_0$  states.<sup>35, 36</sup> Note however that at threshold (i.e. 0 eV kinetic energy), neither process is expected to contribute to the photoelectron spectrum.<sup>29</sup> Alternatively, it could suggest that the adiabatic detachment energy is actually somewhat lower than what we measure from the extrapolation of the photoelectron feature in Fig. 2. Specifically, the fact that the tail of the thermionic emission extends to  $\sim 0.2$  eV would suggest that the adiabatic energy may be as low as 2.38 eV, which would be in agreement with theory.<sup>23</sup> However, given the laser bandwidth and the finite temperature, this seems unlikely.

Our observations are consistent with those of the Jockusch<sup>13, 14</sup> and Andersen<sup>11, 12</sup> groups. A major channel that is observed in both these studies is fragmentation. Jockusch and co-workers also observe an electron loss channel at 480 nm and, through power-dependence studies, they have attempted to determine the process of electron detachment by considering the numbers of photons absorbed. Here, we have shown that following internal

conversion, in addition to multiple-photon absorption, thermionic emission can be observed. At higher excitation energies, direct and autodetachment also contribute, although we cannot determine their relative contributions. Taking this together with the fact that no fluorescence is observed in the gas-phase from  $S_1$  excited HBDI<sup>-</sup>, strongly points to internal conversion as the dominant decay channel for the  $S_1$  state excited at 480 nm. This paves the way for studies that monitor the decay dynamics in real-time using time-resolved photoelectron spectroscopy and these experiments are underway in our laboratory.

## Conclusions

The photoelectron spectroscopy of the GFP anionic chromophore HBDI<sup>-</sup> is presented. The vertical detachment energy is determined to be  $2.8 \pm 0.1$  eV and is higher than the  $S_1 \leftarrow S_0$  absorption maximum in the gas-phase. This indicates that, upon excitation of the  $S_1$  state, autodetachment is not expected to be a dominant channel in the Franck-Condon region. This is further evidenced by the photoelectron spectrum taken at 2.58 eV, which is resonant with the  $S_1 \leftarrow S_0$  transition. This shows clear evidence for thermionic emission of electrons, indicating that internal conversion to the anionic ground state is an important deactivation channel following  $S_1 \leftarrow S_0$  excitation. The photoelectron spectrum taken at 6.15 eV shows the presence of several excited states of the neutral radical of HBDI. These have been assigned using TD-DFT calculations to the formation of holes in successively lower lying MOs of the anion, providing a detailed experimental probe into the electronic structure of the anion which will serve as a further benchmark for theoretical investigations.

## Acknowledgements

The authors thank Dr. S. L. Cobb for synthesis of HBDI, Prof. D. J. Tozer, Dr. G.M. Roberts and Dr. A. Beeby for assistance and useful discussions regarding TD-DFT and Dr. E. Wrede for loan of the Nd:YAG system. We also thank Prof. R. A. Jockusch for sharing their action spectra data of HBDI<sup>-</sup>. This work has been supported by the EPSRC (EP/D073472/1) and the University of Durham.

## Notes and references

- <sup>a</sup> Dept. of Chemistry, University of Durham, South Road, DH1 3LE, Durham, United Kingdom; E-mail: j.r.r.verlet@durham.ac.uk  
† Electronic Supplementary Information (ESI) available: Details on: Calibration of photoelectron spectra; effect of internal energy on photoelectron spectra; electronic structure calculations; Simulation of photoelectron spectra; power dependence of 480 nm spectra. See DOI: 10.1039/b000000x/
1. R. Y. Tsien, *Annu. Rev. Biochem.*, 1998, **67**, 509-544.
  2. M. Zimmer, *Chem. Rev.*, 2002, **102**, 759-782.
  3. S. R. Meech, *Chem. Soc. Rev.*, 2009, **38**, 2922-2934.
  4. V. Sample, R. H. Newman and J. Zhang, *Chem. Soc. Rev.*, 2009, **38**, 2852-2864.
  5. R. Heim, D. C. Prasher and R. Y. Tsien, *Proc. Natl. Acad. Sci. U. S. A.*, 1994, **91**, 12501-12504.
  6. M. Chattoraj, B. A. King, G. U. Bublitz and S. G. Boxer, *Proc. Natl. Acad. Sci. U. S. A.*, 1996, **93**, 8362-8367.
  7. G. H. Patterson, S. M. Knobel, W. D. Sharif, S. R. Kain and D. W. Piston, *Biophys. J.*, 1997, **73**, 2782-2790.

8. G. Bublitz, B. A. King and S. G. Boxer, *J. Am. Chem. Soc.*, 1998, **120**, 9370-9371.
9. H. Niwa, S. Inouye, T. Hirano, T. Matsuno, S. Kojima, M. Kubota, M. Ohashi and F. I. Tsuji, *Proc. Natl. Acad. Sci. U. S. A.*, 1996, **93**, 13617-13622.
10. N. M. Webber, K. L. Litvinenko and S. R. Meech, *J. Phys. Chem. B*, 2001, **105**, 8036-8039.
11. S. B. Nielsen, A. Lapierre, J. U. Andersen, U. V. Pedersen, S. Tomita and L. H. Andersen, *Phys. Rev. Lett.*, 2001, **87**, 228102.
12. L. H. Andersen, A. Lapierre, S. B. Nielsen, I. B. Nielsen, S. U. Pedersen, U. V. Pedersen and S. Tomita, *Eur. Phys. J. D*, 2002, **20**, 597-600.
13. M. W. Forbes and R. A. Jockusch, *J. Am. Chem. Soc.*, 2009, **131**, 17038-17039.
14. M. W. Forbes, A. M. Nagy and R. A. Jockusch, *Int. J. Mass Spectrom.*, 2011, **308**, 155-166.
15. A. Sanov and R. Mabbs, *Int. Rev. Phys. Chem.*, 2008, **27**, 53 - 85.
16. J. R. R. Verlet, *Chem. Soc. Rev.*, 2008, **37**, 505-517.
17. J. Lecointre, G. M. Roberts, D. A. Horke and J. R. R. Verlet, *J. Phys. Chem. A*, 2010, **114**, 11216-11224.
18. D. A. Horke and J. R. R. Verlet, *Phys. Chem. Chem. Phys.*, 2011, **13**, 19546-19552.
19. S. Kojima, H. Ohkawa, T. Hirano, S. Maki, H. Niwa, M. Ohashi, S. Inouye and F. I. Tsuji, *Tetrahedron Lett.*, 1998, **39**, 5239-5242.
20. A. T. J. B. Eppink and D. H. Parker, *Rev. Sci. Instrum.*, 1997, **68**, 3477-3484.
21. G. M. Roberts, J. L. Nixon, J. Lecointre, E. Wrede and J. R. R. Verlet, *Rev. Sci. Instrum.*, 2009, **80**, 053104.
22. A. V. Nemukhin, B. L. Grigorenko and A. P. Savitskya, *Acta Natur.*, 2009, **2**, 33-43.
23. E. Epifanovsky, I. Polyakov, B. Grigorenko, A. Nemukhin and A. I. Krylov, *J. Chem. Theory Comput.*, 2009, **5**, 1895-1906.
24. E. Epifanovsky, I. Polyakov, B. Grigorenko, A. Nemukhin and A. I. Krylov, *J. Chem. Phys.*, 2010, **132**, 115104.
25. D. A. Horke, A. S. Chatterley and J. R. R. Verlet, *J. Phys. Chem. Lett.*, 2012, **3**, 834-838.
26. X.-B. Wang and L.-S. Wang, *Rev. Sci. Instrum.*, 2008, **79**, 073108.
27. T. Yanai, D. P. Tew and N. C. Handy, *Chem. Phys. Lett.*, 2004, **393**, 51-57.
28. M. J. Frisch, G. W. Trucks, H. B. Schlegel, G. E. Scuseria, M. A. Robb, J. R. Cheeseman, G. Scalmani, V. Barone, B. Mennucci, G. A. Petersson, H. Nakatsuji, M. Caricato, X. Li, H. P. Hratchian, A. F. Izmaylov, J. Bloino, G. Zheng, J. L. Sonnenberg, M. Hada, M. Ehara, K. Toyota, R. Fukuda, J. Hasegawa, M. Ishida, T. Nakajima, Y. Honda, O. Kitao, H. Nakai, T. Vreven, J. J. A. Montgomery, J. E. Peralta, F. Ogliaro, M. Bearpark, J. J. Heyd, E. Brothers, K. N. Kudin, V. N. Staroverov, R. Kobayashi, J. Normand, K. Raghavachari, A. Rendell, J. C. Burant, S. S. Iyengar, J. Tomasi, M. Cossi, N. Rega, J. M. Millam, M. Klene, J. E. Knox, J. B. Cross, V. Bakken, C. Adamo, J. Jaramillo, R. Gomperts, R. E. Stratmann, O. Yazyev, A. J. Austin, R. Cammi, C. Pomelli, J. W. Ochterski, R. L. Martin, K. Morokuma, V. G. Zakrzewski, G. A. Voth, P. Salvador, J. J. Dannenberg, S. Dapprich, A. D. Daniels, Ö. Farkas, J. B. Foresman, J. V. Ortiz, J. Cioslowski and D. J. Fox, *Gaussian09, Revision A.02*, (2009) Gaussian, Inc., Wallingford CT.
29. E. P. Wigner, *Phys. Rev.*, 1948, **73**, 1002-1009.
30. B. Baguenard, J. C. Pinaré, C. Bordas and M. Broyer, *Phys. Rev. A*, 2001, **63**, 023204.
31. B. Baguenard, J. C. Pinaré, F. Lépine, C. Bordas and M. Broyer, *Chem. Phys. Lett.*, 2002, **352**, 147-153.
32. K. Hansen, K. Hoffmann and E. E. B. Campbell, *J. Chem. Phys.*, 2003, **119**, 2513-2522.
33. M. Kjellberg, O. Johansson, F. Jonsson, A. V. Bulgakov, C. Bordas, E. E. B. Campbell and K. Hansen, *Phys. Rev. A*, 2010, **81**, 023202.
34. C. E. Klots, *Z. Phys. D: At., Mol. Clusters*, 1991, **20**, 105-109.
35. I. V. Polyakov, B. L. Grigorenko, E. M. Epifanovsky, A. I. Krylov and A. V. Nemukhin, *J. Chem. Theory Comput.*, 2010, **6**, 2377-2387.
36. M. E. Martin, F. Negri and M. Olivucci, *J. Am. Chem. Soc.*, 2004, **126**, 5452-5464.